Phytomedicine 149 (2025) 157580

Contents lists available at ScienceDirect

Phytomedicine

journal homepage: www.elsevier.com/locate/phymed

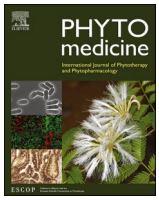

Original Article

Timosaponin B-II attenuates cerebral ischemia injury by enhancing Parkin-mediated mitophagy

Yueyang Liu [a,1], Hanxiao Shang [b,1], Lu Zhang [a,1], Rong Fu [a], Yayi Li [a], Zhuo Wang [a,c], Yanru Zhen [a], Qi Zhang [a], Yang Zhao [b,*], Guannan Wang [d,*], Ming-Sheng Zhou [a,*]

[a] *Shenyang Key Laboratory of Vascular Biology, Science and Experimental Research Center of Shenyang Medical College, No. 146 Huanghe North Street, Yuhong District, Shenyang 110034, PR China*
[b] *Department of Pharmacology, Shenyang Pharmaceutical University, Shenyang 110016, PR China*
[c] *General Hospital of Northern Theater Command, Shenyang 110003, PR China*
[d] *Shenyang Key Laboratory of Medical Molecular Theranostic Probes in School of Pharmacy, Shenyang Medical College, Shenyang 110034, PR China*

ARTICLE INFO

Keywords:
Ischemic stroke
Mitophagy
Parkin
Timosaponin B-II
Oxidative stress

ABSTRACT

Background: Ischemic stroke (IS) is linked to dysregulated mitophagy. Timosaponin B-II (TBII), a complex furostan steroid saponin extracted from *Anemarrhena asphodeloides* Bunge, has been demonstrated to play a crucial role in regulating autophagy. However, whether TBII exerts therapeutic effects in cerebral ischemia through the regulation of autophagy, particularly Parkin-dependent pathways remained unexplored.
Purpose: The present study investigated whether TBII can alleviate cerebral ischemic injury by enhancing Parkin-dependent mitophagy.
Methods: We evaluated TBII's effects on cerebral ischemic injury using permanent middle cerebral artery occlusion (pMCAO) in mice and oxygen-glucose deprivation (OGD)-treated neurons. Mitophagy and mitochondrial function were assessed by Western blot, transmission electron microscopy (TEM), and immunofluorescence techniques. Parkin knockdown (sh*Prkn* lentivirus) and the mitophagy inhibitor Mdivi-1 were employed to validate TBII' mechanisms.
Results: Intragastrical (i.g.) administration of TBII (10, 20, 40 mg/kg) for 7 days significantly reduced cerebral infarction volume, brain water content, and neurological deficits in pMCAO mice, while attenuating neuronal death in *vivo* and *in vitro*. Molecular docking, cellular thermal shift assays (CETSA), drug affinity responsive target stability (DARTS), and molecular dynamics simulations confirmed that TBII specifically binds and stabilizes to Parkin, suggesting its potential to enhance mitophagy. TBII mitigated the impairment of mitophagy by upregulating Parkin and p-Parkin (Ser65), promoting the ubiquitination of mitochondria, the degradation of autophagy substrate SQSTM1 and damaged mitochondria after IS. TBII also preserved mitochondrial membrane potential (MMP), suppressed oxidative stress, and restored mitochondrial function and ultrastructure. These benefits were reversed by the mitophagy inhibitor Mdivi-1 and Parkin knockdown.
Conclusion: The present study demonstrates that TBII reduces oxidative stress, preserves mitochondrial function, and ultimately attenuates ischemic brain injure by enhancing Parkin-dependent mitophagy. Our study provides the first evidence supporting TBII as a promising therapeutic agent for IS.

Abbreviations: 8-OHdG, 8-hydroxy-2′-deoxyguanosine; CETSA, cellular thermal shift assays; DAPI, 4′,6-diamidino-2-phenylindole; DARTS, drug affinity responsive target stability; DMEM, Dulbecco's modified Eagle's medium; GSH, glutathione; H2O2, hydrogen peroxide; i.g., intragastrical; IS, ischemic stroke; MDA, malondialdehyde; MMP, mitochondrial membrane potential; mNSS, modified neurological severity score; mTOR, mammalian target of rapamycin; NBP, butylphthalide; NF-κB, nuclear factor κB; OGD, oxygen-glucose deprivation; pMCAO, permanent middle cerebral artery occlusion; RMSD, root mean square deviation; MSF, root mean square fluctuation; SOD, superoxide dismutase; TBII, timosaponin B-II; TEM, transmission electron microscopy.

* Corresponding authors.
E-mail addresses: zhaoyangzoey@163.com (Y. Zhao), chemwangguannan@symc.edu.cn (G. Wang), zhoums@symc.edu.cn (M.-S. Zhou).
[1] These authors contributed equally to this work.

https://doi.org/10.1016/j.phymed.2025.157580
Received 27 June 2025; Received in revised form 2 November 2025; Accepted 20 November 2025
Available online 24 November 2025

Background

Ischemic stroke (IS) remains a predominant cause of global mortality and permanent disability. Its pathophysiology is initiated by a critical reduction in cerebral blood flow followed by arterial occlusion, which rapidly depletes the oxygen and glucose supplies essential for neuronal survival. This energy failure triggers a complex deleterious cascade of events, beginning with excitotoxic glutamate release, ionic imbalance and mitochondria dysfunction, which swiftly propagate to secondary injury mechanisms, including excessive oxidative stress, neuroinflammation. These processes consequently activate cell death pathways, such as cell necrosis, apoptosis, and autophagy, ultimately leading to cerebral infarction and alterations in neurobehavioral function (Duan et al., 2025; Qin et al., 2022). Despite our understanding of these core mechanisms, the intricate and overlapping nature of this injury cascade has complicated the development of successful pharmacological interventions, highlighting a critical unmet need in IS therapy (Majumder, 2024).

Autophagy is a biological process through which cells utilize lysosomes to degrade proteins and damaged organelles, collectively referred to as the autophagy-lysosomal pathway (Nixon and Rubinsztein, 2024). Increasing evidence indicate that autophagy is predominantly activated in neurons following IS, where it protects neurons from ischemic injury (Liu et al., 2024; Wu et al., 2025b). However, we have previously demonstrated that IS can induce lysosomal dysfunction, thereby impairing autophagic flux (Liu et al., 2024). Mitophagy, a selective form of autophagy, mediates the lysosomes-dependent clearance of damaged mitochondria. When mitophagy is impaired, damaged mitochondria fail to undergo degradation and accumulate in the cytoplasm, triggering mitochondrial-mediated oxidative stress and apoptosis (Lu et al., 2023). This process ultimately exacerbates cerebral ischemic injury. Conversely, enhanced mitophagy has been shown to confer protective effects against ischemic injury (Li et al., 2023a; Meng et al., 2025b).

The PINK1/Parkin pathway is a central regulator of mitophagy. Upon mitochondrial damage and depolarization, Parkin is recruited to the mitochondria via PINK1, where it ubiquitinates outer membrane proteins through its E3 ligase activity. These ubiquitinated proteins are recognized by adaptor proteins such as SQSTM1, which bind to LC3 on autophagosomal membranes via LC3-interacting regions. This process enables the selective engulfment and degradation of damaged mitochondria, completing mitophagy (Connelly et al., 2023; Li et al., 2023b). Mounting evidence indicates that cerebral ischemia suppresses Parkin expression, impairing mitophagy and leading to damaged mitochondrial accumulation (Sun et al., 2022; Tang et al., 2016; Wen et al., 2021). Conversely, enhancing Parkin expression has been shown to restore mitophagy quality control and mitigate cerebral ischemic injury (Sun et al., 2022; Wen et al., 2021; Wu et al., 2021a). These findings suggest that enhancement of Parkin-mediated mitophagy may hold promise as a potential therapeutic strategy against ischemic injury.

The rhizome of *Anemarrhena asphodeloides* Bunge, has long been used in Chinese traditional medical recipes for the treatment of various inflammatory diseases (Liu et al., 2022; Lu et al., 2009; Zhang et al., 2015). Recent studies suggest that sapogenins derived from *A. asphodeloides*, particularly timosaponin A-III (TAIII) and timosaponin B-II (TBII), exhibit significant therapeutic effects for central nervous system (CNS) diseases (Chen et al., 2020; Lee et al., 2009; Li et al., 2007). These neuroprotective effects may be attributed to its anti-inflammation and antioxidant properties. Notably, emerging studies have demonstrated that timosaponin plays a crucial role in regulating autophagy. Mechanistic studies reveal that TBII dose-dependently inhibits osteoblast apoptosis through the inhibition of the mammalian target of rapamycin (mTOR) and nuclear factor κB (NF-κB) signaling pathway, thereby activating autophagy (Wang et al., 2021). Similarly, TAIII can enhance autophagic flux by stimulating the formation of autophagosomes and their maturation into autolysosomes: a process linked to mTOR inhibition and increased cytoplasmic free calcium levels (Lok et al., 2011). However, whether timosaponin improves cerebral ischemic injury by regulating autophagy remains unexplored.

In this study, we investigated whether TBII confers protection against cerebral ischemia. Using molecular docking, cellular thermal shift assays (CETSA), drug affinity responsive target stability (DARTS) and molecular dynamics simulation assays, we demonstrated that TBII likely modulates Parkin-mediated mitophagy. Building on this finding, we further investigated the effects of TBII on mitochondrial function and ischemic injury following IS. Our works provide the first evidence that TBII attenuates cerebral ischemic injury by enhancing Parkin-mediated mitophagy.

Materials and methods

Animals and ethics statement

Male C57BL/6 mice were obtained from the Liaoning Changsheng Biotechnology Inco (China). The mice were housed under standard conditions (12 h light-12 h dark cycle, 25°C) with free access to food and tap water. All experimental procedures and treatments adhered to the National Institutes of Health Guide for the Care and Use of Laboratory Animals (NIH Publication No. 8023, revised 1978) and were approved by the Experimental Animals Ethics Committee of Shenyang Medical College (Approval No. SYXY2023090101 [Sep. 1, 2023], Shenyang, China).

Experimental design and grouping

Pharmacodynamic evaluation of TBII protection on cerebral ischemia: A total of 78 mice were used. After excluding 11 mice that died from surgery and 7 that did not meet inclusion criteria, the remaining 60 mice were randomly assigned to the following groups (n = 7-8/group): Sham, permanent middle cerebral artery occlusion (pMCAO)+ Vehicle, pMCAO + TBII (5, 10, 20, 40, 80 mg/kg), and pMCAO + NBP (80 mg/kg, positive control). TBII was dissolved in saline and intragastrically (i.g.) administered once daily for 7 days before pMCAO operation. The dosage of TBII was selected based on existing literature (Deng et al., 2015; Li et al., 2007; Xing et al., 2020; Zhao et al., 2016) and established safety profiles (Lin et al., 2017). In addition, we selected butylphthalide (NBP) as a positive control due to its established efficacy in IS, since it shared oral administration route with TBII. NBP (80 mg/kg, i.g.) was dissolved in oil and administered once daily for 7 days before pMCAO (Meng et al., 2025a; Wu et al., 2025a). An additional group of 196 mice were used for investigating the mechanisms of TBII alleviation of cerebral ischemia. After excluding 24 mice that died during surgery and 18 that were disqualified, 154 mice were randomly divided into the following groups (n = 29-32/group): Sham; pMCAO + Vehicle; pMCAO + TBII (10, 20, 40 mg/kg).

Evaluation of TBII efficacy with Mdivi-1 cotreatment: A total of 52 mice (22-25 g) were used. After excluding 9 mice that died during surgery and 9 that did not meet criteria, 34 mice were randomly allocated to the following groups (n = 5-6/group): Sham, Sham + Mdivi-1, pMCAO + Vehicle; pMCAO + Mdivi-1; pMCAO + TBII (40 mg/kg), pMCAO + TBII + Mdivi-1. Mdivi-1 (3 mg/kg) was dissolved in saline and administered by intraperitoneal (i.p.) injection immediately following pMCAO induction (Zhang et al., 2013).

Evaluation of TBII efficacy with LV-sh*Prkn* knockdown: A total of 44 mice (18–20 g) were used. After excluding 9 mice that died during surgery and 4 that were disqualified, 31 mice were randomly assigned to the following groups (n = 7-9/group): Sham + LV-sh*Scr*, pMCAO + LV-sh*Scr*, pMCAO + TBII + LV-sh*Scr*, and pMCAO + TBII + LV-sh*Prkn*.

Drugs and reagents

TBII was purchased from Beijing Zhongke Quality Inspection Biotechnology Co., Ltd., Beijing, China, with a purity exceeding 98%.

NBP soft capsules were purchased from Shijiazhuang Group Enbipu Pharmaceutical Co., Ltd., Shijiazhuang, China. Mdivi-1 was obtained from Selleck Co., Ltd., Houston, TX, USA (S7162).

Establishment of pMCAO model

The pMCAO model was induced as previously described by Longa et al. (1989). Mice were fasted for 12 h with free access to water before surgery. Animals were randomly assigned into either the sham- or pMCAO-operated group. Mice were anesthetized via inhalation of isoflurane (1.5% vol./vol.) in air (RWD Life Science, Shenzhen, China). A ventral midline incision was made to expose the right common carotid artery, external carotid artery, and internal carotid artery. The common carotid artery and external carotid artery were permanently ligated, and the internal carotid artery was temporarily occluded using a metal micro-vessel clip. A silicon-coated nylon filament was inserted through the right common carotid artery into the lumen of the right internal carotid artery until it reached the origin of the middle cerebral artery at the circle of Willis to achieve permanent occlusion. Sham-operated mice underwent same surgical procedures except for filament insertion and middle cerebral artery occlusion. Mice with a cerebral blood flow reduction of less than 60% at 24 h post-pMCAO were excluded from subsequent analyses.

Assessment of cerebral blood flow

CBF was measured at baseline, and at 30 min, 3 h, and 24 h post-pMCAO using the RFLSI Pro laser speckle imaging system (RWD Life Science Co., Ltd.). Mice were anesthetized with isoflurane-O_2 and positioned in a stereotaxic frame in the prone position. The scalp was incised to expose the skull. Laser speckle blood flow images were acquired, and cerebral blood flow was quantified within the same region of interest (ROI) in the right hemisphere.

Assessment of cerebral infarct volume, brain water content and neurological function

To measure brain infarct volume, mice were euthanized at 24 h post-pMCAO, and their brains were immediately removed and sliced into six coronal sections at 2-mm intervals. The sections were stained with a 1% solution of 2, 3, 5-triphenyltetrazolium chloride (TTC; Sigma-Aldrich, St. Louis, MO, USA, T8877) at 37°C for 30 min and subsequently fixed with 4% paraformaldehyde. Photographic images were captured, and the infarcted areas were quantified using Pro Plus software (version 6.0). Infarct volume was calculated as follows: Infarct volume (%) = [contralateral hemisphere volume − (ipsilateral hemisphere volume − infarct volume)] / contralateral hemisphere volume × 100% (Liu et al., 2021, 2023). Subsequently, the slices were dried at 65°C for 96 h and weighed accurately. Brain water content, as an indicator of cerebral edema, was determined using the wet/dry method as previously described. Neurological function was assessed using the modified neurological severity score (mNSS) test, where each function is scored on a scale of 0-18 (normal score, 0; maximal deficit score, 18). Higher scores indicate more severe behavioral deficits (Liu et al., 2023).

Grid walk test

Mice were tested on an elevated metal grid (60 × 50 cm) with individual mesh openings of 10 × 10 mm. Each mouse was placed at the center of the grid, and its locomotor activity was recorded using a video camera to accurately capture instances of missteps during the trial. The duration of the test was 2 min. Fault assessment was conducted by reviewing the recorded video footage to count both the total number of steps taken by the right forelimb and right hindlimb, as well as the number of foot slips that occurred. A foot fault was defined as any instance where the limb failed to securely contact the grid surface, slipped into a grid aperture, lost grip due to insufficient support, or the hindlimb remained within a grid hole. The error rate was calculated using the following formula: % of foot fault = (number of slips/ total number of steps over 2 min) × 100% (Ye et al., 2020).

Immunofluorescence

At 24 h post-pMCAO, the animals were perfused with PBS (ZSGB-BIO, ZLI-9061, Beijing, China) followed by 4% paraformaldehyde (PFA, Beyotime Biotechnology, P0099, Shanghai, China). Serial coronal brain sections were cut on vibratome (Leica, VT1000S, Wetzlar, Germany) with 40 μm thickness. Antigen was retrieved by incubating with the retrieval solution (ZSGB-BIO, ZLI-9065) at 85°C for 30 min. The sections were incubated with 5% PBS-goat serum (ZSGB-BIO, ZLI-9056) containing 0.3% Triton X-100 for 1 h, and subsequently incubated overnight at 4°C with the primary antibodies against anti-LC3 rabbit pAb (1:200; Medical Biological Laboratories, PM036, Kyoto, Japan), anti-NeuN mouse mAb (1:500; Millipore, MAB377, Burlington, MA, USA), anti-TOMM20 mouse mAb (1:500, Abcam, ab56783, Cambridge, UK), overnight at 4°C. After incubation, samples were washed three times with PBS and incubated for 1 h at room temperature with fluorochrome-coupled goat-anti rabbit and goat anti-mouse secondary antibodies (1:200; Alexa Fluor 488; 555; Beyotime Biotechnology, A0428; A0516). The nuclei were counterstained with DAPI. Confocal images were acquired using a Nikon Ni-E confocal microscope (Nikon Instruments Inc., Tokyo, Japan) equipped with an A1R scanner (Nikon), a 60x objective (Nikon), a 130 W metal halide lamp (Nikon), and a laser device (Coherent Inc., Santa Clara, CA, USA). Fluorophores were excited 405 nm (50 mW), 488 nm (50 mW), and 561 nm (50 mW). All images were blindly acquired across experimental groups under the same laser power, pinhole and gain, and were analyzed with Image J (NIH, version 2.0) without adjusting image brightness or contrast.

Transmission electron microscopy (TEM)

At 24 h post-pMCAO, mice were perfused with a modified fixative containing 2% paraformaldehyde and 2.5% glutaraldehyde (Damao chemical reagent factory, Tianjin, China) in phosphate buffer (pH 7.4). The cortex was microdissected into 1 mm^3 blocks. Samples were placed in 2.5% glutaraldehyde fixation solution followed by post-fixation in osmium tetroxide (Zhongjingkeyi Technology, Beijing, China). Subsequently, samples were dehydrated in a graded ethanol series, embedded in araldite (Zhongjingkeyi Technology), and aggregated into a solid. Then the solid was cut into ultrathin sections (70 nm) and stained with uranyl acetate (Zhongjingkeyi Technology) and lead citrate (Zhongjingkeyi Technology). Images were acquired using a TEM (Chiyoda, Tokyo, Japan).

Cell culture and establishment of oxygen-glucose deprivation (OGD) model

The HT22 cells were obtained from the National Collection of Authenticated Cell Cultures (Shanghai, China) and cultured in Dulbecco's Modified Eagle's Medium (DMEM, Gibco, Grand Island, NY, USA C11965500BT) supplemented with 10% fetal bovine serum and 1% penicillin-streptomycin solution. For the experiments, cells were grown in a humidified incubator (5% CO_2, 37°C) and passaged when reaching 70% confluency. Cells were placed on culture plates or dishes and were fed fresh medium overnight, for subsequent experiments. To establish the OGD model, The culture medium was replaced with glucose-free DMEM. Then cells were transferred to a hypoxic chamber filled with 95% N_2 and 5% CO_2 at the indicated time points. HT22 cells were incubated with different concentrations of TBII (0.1, 0.3, 1, 3, 10, 30, 100 μM) (Lu et al., 2009; Xing et al., 2020), NBP (10 μM) (Mi et al., 2024) or Mdivi-1 (1 μM) (Zhang et al., 2013) for 2 h prior to OGD exposure. Treatments were maintained in glucose-free DMEM throughout the indicated OGD exposure period. TBII, NBP and Mdivi-1

were first dissolved in DMSO as a stock solution and subsequently diluted with the cell culture medium immediately before application.

Cell viability

Cell viability was assessed using an MTT assay. At 12 h after OGD exposure, the cells were incubated with 20 μl of MTT solution (5 mg/ml; Sigma-Aldrich, M5655) for 4 h. Following incubation, the medium was removed, and the formed formazan crystals were dissolved in 200 μl of DMSO (Sigma-Aldrich, D2650). The absorbance was measured at 560 nm to determine cell viability.

Western blotting

Total proteins were extracted from brain tissue and cells using radioimmunoprecipitation assay buffer (Beyotime Biotechnology, P0013B,) supplemented with a protease inhibitor cocktail. A mitochondrial extraction kit (Beyotime Biotechnology, C3606, C3601) was used for isolating mitochondrial protein. Proteins were separated by SDS-PAGE and transferred onto polyvinylidene fluoride membranes (Millipore, IPVH00010, Billerica, MA, USA), followed by incubation with blocking buffer containing 5% skimmed milk (Becton Dickinson, 232100, NJ, USA) for 1 h at room temperature. The membranes were then incubated overnight at 4°C with the following primary antibodies: anti-GAPDH rabbit pAb (1:1000; Elabscience, E-AB-40338, Wuhan, Hubei, China), anti-TOMM20 mouse mAb (1:1000; Abcam, ab56783), anti-Parkin rabbit pAb (1:1000; Cell Signaling Technology, 2132, Danvers, MA, USA), anti-PINK1 rabbit pAb (1:1000; Proteintech, 23274-1-AP, Wuhan, Hubei, China), anti-LC3 rabbit pAb (1:500; Medical Biological Laboratories, PM036), anti-SQSTM1/p62 mouse mAb (1:2000; Abcam, ab56416), anti-phospho-Parkin (Ser65) rabbit pAb (1:1000; Affinity Biosciences, AF3500, Cincinnati, OH, USA), anti-ubiquitin mouse mAb (1:500; Santa Cruz Biotechnology, sc-8017, Dallas, TX, USA), anti-NIX rabbit mAb (1:1000; Cell Signaling Technology, 12396), anti-FUNDC1 rabbit pAb (1:1000; Abcam, ab224722), anti-BNIP3 mouse mAb (1:10000; Proteintech, 68091-1-lg) and anti-VDAC1 rabbit pAb (1:1000; Affinity Biosciences, DF6140). After washing, the membranes were incubated with HRP-goat anti-rabbit and HRP-goat anti-mouse secondary antibodies (1:5000; ZSGB-BIO, ZB-2301, ZB-2305) at room temperature for 1 h. Subsequently, the membranes were exposed to ECL reagents (Thermo Fisher Scientific, 34580, Waltham, MA, USA) for visualization. Protein expressions were quantified using densitometric analysis performed with ImageJ software (version 2.0).

JC-1 staining

The cellular MMP was evaluated using fluorescent probe JC-1 (Beyotime Biotechnology, C2003S). After 12 h of OGD treatment, cells were washed with PBS and incubated with JC-1 solution for 30 min at 37°C, fluorescence was measured using a fluorescence microscope with dual emission detection: JC-1 aggregates were detected at 490/530 nm and JC-1 monomers at 525/590 nm.

Determination of reactive oxygen species with dichlorodihydrofluorescein diacetate assay (DCFH-DA) and MitoSox staining

Cellular reactive oxygen species levels were quantified using the DCFH-DA (Beyotime Biotechnology, S0033M). At 12 h of OGD exposure, cells were incubated with DCFH-DA (10 μM) at room temperature for 30 min. Fluorescent intensity was measured at an emission wavelength of 500 nm and an excitation wavelength of 525 nm. Mitochondrial reactive oxygen species levels were determined using MitoSox-red (Thermo Fisher Scientific, M36008). Cells were incubated with MitoSox-red (1 μM) at room temperature for 30 min. After staining, cells were visualized using fluorescence microscopy.

Assessments of superoxide dismutase (SOD), malondialdehyde (MDA), 8-hydroxy-2′-deoxyguanosine (8-OHdG), glutathione (GSH), and hydrogen peroxide (H_2O_2)

For *in vitro* experiments, cells were collected and centrifuged to obtain supernatants at 12 h after OGD exposure. For *in vivo* experiments, the ipsilateral cortex was homogenized and centrifuged to obtain supernatants at 24 h post-pMCAO. All assays were performed according to the manufacturer's protocols using the following kits (Beyotime Biotechnology): SOD activity assay kit (S0101S), lipid peroxidation MDA assay kit (S0131M), 8-OHdG (ab285254, Abcam), GSH assay kit (S0053), and H_2O_2 assay kit (S0038).

Detection of ATP

Intracellular ATP quantification was measured using a commercial kit (Beyotime Biotechnology, S0026). Briefly, after 12 h of OGD exposure, cell lysates were centrifuged to collect supernatants. Following the manufacturer's protocol, 100 μl of ATP detection solution was added to each well of a 96-well plate. Then, 20 μl of sample supernatant was added to the wells and mixed immediately. The luminescence was measured using a luminometer, and ATP concentrations were determined based on a standard curve.

Lentiviral (LV) transfection

A selected shRNA sequence targeting mouse Parkin was inserted into a LV to knockdown Parkin. The recombinant LV construct (pSLenti-U6-sh*RNA (Prkn)*-CMV-EGFP-F2A-Puro-WPRE) was packaged by Obio Technology Company (Shanghai, China). The target shRNA sequence is GCTGGGACGATGTCTTAATTC. For *in vitro* knockdown, HT22 cells were transfected with LV for 12 h, after which the medium was replaced. Cells then were incubated for an additional 60 h. For *in vivo* knockdown, mice were anesthetized with isoflurane, and LV particles were stereotactically injected into the cerebral cortex. Specifically, a total of 1 μl of LV particles were injected across three cortical sites using a 33G Hamilton syringe with an automatic injector at a rate of 0.25 μl/min: The three-dimensional coordinates of two sites were: Site 1: AP -0.5 mm, - ML +1.25 mm and DV 1.5 mm; Site 2: ML +2.25 mm, AP+0.94 mm and DV 1.5 mm. The needle was retained in place for 5 min after injection completion to prevent backflow, then retracted slightly and held for an additional 2 min before removal. Mice were allowed to recover for 3 weeks before pMCAO.

Molecular docking

The structure of TBII was constructed using ChemDraw. The crystal structures of protein were downloaded from the Protein Data Bank. Then the obtained protein structures and TBII structure were introduced into Autodock. The protein structures were prepared for docking by removing water molecules and adding hydrogens. The docking process was performed by the algorithm. The top scored binding models was chosen to visualize the interactions between Parkin (PDB ID: 6GLC) and TBII.

Molecular dynamics simulation

Molecular dynamics simulations (300 ns) for Parkin and Parkin-TBII were performed using GROMACS 2022. Systems were built using charmm36 force field in dodecahedral boxes ($\geq$1 nm edge), solvated with TIP3P water and neutralized by Na^+/Cl^-. After NVT equilibration (200 ps, 1 fs step) at 310 K (V-rescale, τ=0.1 ps), NPT stabilization (500 ps, 2 fs step) at 1 atm (Parrinello-Rahman, τ=2 ps) was conducted. Long-range electrostatics used PME (0.16 Å grid, 1.3 nm cutoff), with bond constraints applied via LINCS.

DARTS assay

The cells were scraped and lysed using M-PER lysis buffer (Thermo Fisher Scientific, No. 78501), followed by centrifugation at 4°C. TBII was added and incubated with the mixture for 1 h. Proteolysis was performed by adding pronase (Sigma-Aldrich, No. 11459643001) at dilution ranging from 1:100 to 1:1600 for 13 min. The reaction was immediately terminated by adding protein loading buffer, and boiling at 100°C for 10 min. The samples were loaded onto SDS-PAGE gels for western blot analysis.

CETSA assay

Cells were collected and subjected to three cycles of freeze-thawing using liquid nitrogen to generate lysates. The cell lysates were incubated with TBII for 1 h at room temperature. The mixtures were heated at the designed temperatures (ranging from 37°C to 61°C) for 5 min and then cooled to room temperature. After centrifugation, the soluble fractions were separated by SDS-PAGE and analyzed by western blot.

Statistical analysis

Graphpad Prism software (version 7.0) was used to perform the statistical analysis. The data were expressed as mean ± SEM. Comparisons among three or more groups were analyzed, One-way or Two-way ANOVA, as appropriate, followed by LSD test. The level of significance was set at $P < 0.05$.

Results

Treatment with TBII alleviates ischemic injury and improves neuronal loss after IS

The chemical structure of TBII was shown in Fig. S1. To evaluate the success of the pMCAO model and the effect of TBII on cerebral blood flow, laser speckle was used to measure the cerebral blood flow. The results showed a progressive decrease in cerebral blood flow at 0.5, 3 and 24 h post-pMCAO compared to baseline, confirming the successful establishment of pMCAO model. However, treatment with TBII did not significantly affect cerebral blood flow (Fig. 1A and B). The effect of TBII (5, 10, 20, 40, 80 mg/kg, i.g.) on cerebral infarct volume, brain edema and neurological function were further assessed by TTC staining, brain water content measurement and grid walk test and mNSS, respectively. The results showed that treatment with TBII and NBP significantly decreased the cerebral infarct volume, brain water content (Fig. 1C–E). In addition, TBII and NBP significantly decreased the foot fault and increased the mNSS at 24 h post-pMCAO (Fig. 1F, I). Given that neuronal loss underlies neurological dysfunction, the effects of TBII on neuronal loss, the survival of neurons, was detected *in vivo* and *in vitro*. Immunostaining analysis showed that treatment with TBII significantly increased the NeuN-positive cells in pMCAO-operated mice (Fig. S2A and B). *In vitro*, MTT assay showed that TBII (0.1, 0.3, 1, 3, 10 μM) had no effect on the cell viability in normal control HT22 cells (Fig. 1J), but increased the cell survival following OGD exposure (Fig. 1K). These results suggest that TBII can alleviate ischemic injury and neuronal loss after IS.

TBII reduces oxidative stress after IS

Previous studies have demonstrated that TBII exerts neuroprotective effects in central nervous system diseases through attenuating oxidative stress (Huang et al., 2012; Zhao et al., 2016). To investigate whether the TBII-mediated neuroprotective effects involve oxidative stress reduction, we measured several key markers of oxidant stress and anti-oxidant enzymes. The results showed that pMCAO significantly increased the levels of H_2O_2, MDA and 8-OHdG, while reducing level of antioxidant enzymes GSH and SOD, and these alterations were reversed by TBII (Fig. 2A–E). Similar antioxidant effects were observed in OGD-treated HT22 cells (Fig. 2F–J). These data suggest that the neuroprotective effects of TBII are mediated, at least in part, through reducing oxidative stress.

TBII mitigates mitophagy impairment and enhances mitochondrial function after IS

Mounting evidence indicates that IS impairs mitophagy, and enhancing this process may attenuate the ischemic injury (Sun et al., 2022; Wen et al., 2021; Wu et al., 2021a). As timosaponin has been identified as a potential autophagy modulator (Lok et al., 2011; Wang et al., 2021), we investigated whether TBII can regulate autophagy and mitophagy post-ischemia. Immunostaining analysis showed that pMCAO increased number of neuronal autophagosome, which was further enhanced by TBII treatment (Fig. S2A). Moreover, we observed accumulation of LC3 labeled autophagosomes and TOMM20 labeled mitochondria in pMCAO-operated mice, while treatment with TBII further increased the number of autophagosomes and mitochondria degradation (Fig. 3A–C). TEM was employed to assess TBII's effects on mitophagy in the ipsilateral cortex of mice. Sham-operated mice exhibited a low baseline level of autophagosomes enclosing mitochondria. Treatment with TBII significantly increased the number of autophagosomes engulfing damaged mitochondria following pMCAO (Fig. 3D). Consistent with these findings, Western blot analysis showed that pMCAO increased LC3-II accumulation but decreased Parkin and PINK1 expressions. Treatment with TBII significantly increased LC3-II level, upregulated Parkin and PINK1 expression, coupled with decreased expression of TOMM20 and SQSTM1 (Fig. 3E–J). The effects of TBII on mitophagy was also evaluated in OGD-treated HT22 cells. Similar effects were observed in OGD-treated HT22 cells. Immunofluorescence staining showed that TBII increased LC3 and decrease TOMM20 fluorescence intensity in HT22 cells following OGD (Fig. 4A–C). Western blot analysis showed that TBII increased the expressions of LC3, Parkin and p-Parkin (Ser65), while decreasing SQSTM1 and TOMM20 level in OGD-treated HT22 cells (Fig. 4D–J). Importantly, immunoblot analysis of mitochondrial fraction revealed that TBII enhanced the translocation of LC3, SQSTM1, Parkin, p-Parkin (Ser65) and ubiquitin to mitochondria (Fig. 4K–P). In addition, effects of TBII on receptor-mediated mitophagy were also investigated. The results showed that OGD decreased the NIX and BNIP3 levels but increased FUNDC1 level. However, these changes were not affected by TBII treatment (Fig. S3A–D). Collectively, these results indicate that TBII specifically regulates Parkin-mediated mitophagy by enhancing Parkin's ubiquitin ligase activity and promoting its recruitment to mitochondria.

It is well-known that impaired mitophagy can result in the accumulation of damaged mitochondria, leading to excessive mitochondrial ROS production and exacerbation of cerebral ischemic injury (Li et al., 2023a). To investigate whether TBII enhances mitochondrial function by promoting mitophagy, we performed a serial of mitochondrial assessments. JC-1 staining revealed that TBII concentration-dependently prevented the OGD-induced loss in MMP (Fig. 5A and B). MitoSox staining was used to evaluate the ROS generation in mitochondria. The results showed that the MitoSox fluorescence intensity significantly increased in OGD-treated HT22 cells, an effect was reduced by TBII treatment (Fig. 5C and D). TEM of the ipsilateral cortex showed that mitochondria in sham-operated mice exhibited a fully oval shape with an intact mitochondrial bilayer membrane and well-preserved cristae structure. In contrast, pMCAO induced severe mitochondrial ultrastructural alternations in the ipsilateral cortex, including mitochondrial membrane condensation, cristae loss, organelle shrinkage, occasional mitochondrial rupture. These pathological changes were substantially ameliorated by treatment with TBII (Fig. 5E). Since ATP level is a critical indicator of mitochondrial function, we measured intracellular ATP and found ATP levels were reduced in OGD-treated HT22 cells, and TBII

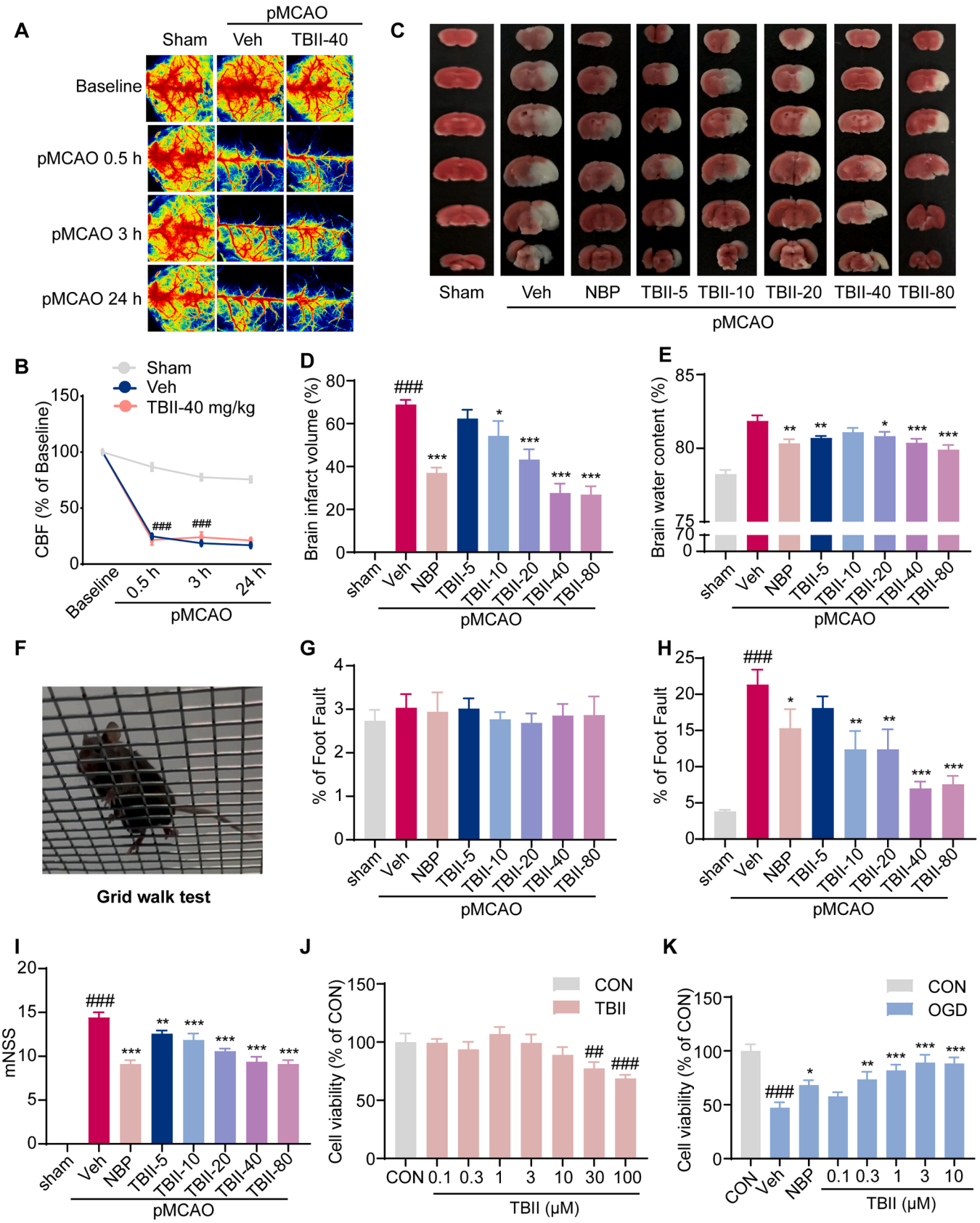

Fig. 1. Timosaponin B-II (TBII) alleviates ischemic injury at 24 h after permanent middle cerebral artery occlusion (pMCAO). Representative images (A) and quantitation (B) of cerebral blood flow (CBF). (C-D) Cerebral infarct volume. (E) Brain water content. Motor function assessed by the grid walk test (F), foot fault rate before (G) and after (H), and mNSS (I) after pMCAO. n=7-8. (J-K) Cell viability in HT22 cells under oxygen-glucose deprivation (OGD). n=6. Data are represented as mean ± SEM. Statistical analysis was performed by one-way ANOVA with LSD test. ###p<0.001, ##p<0.01 vs. Sham or CON group; ***p<0.001, **p<0.01, *p<0.05 vs. pMCAO or OGD group.

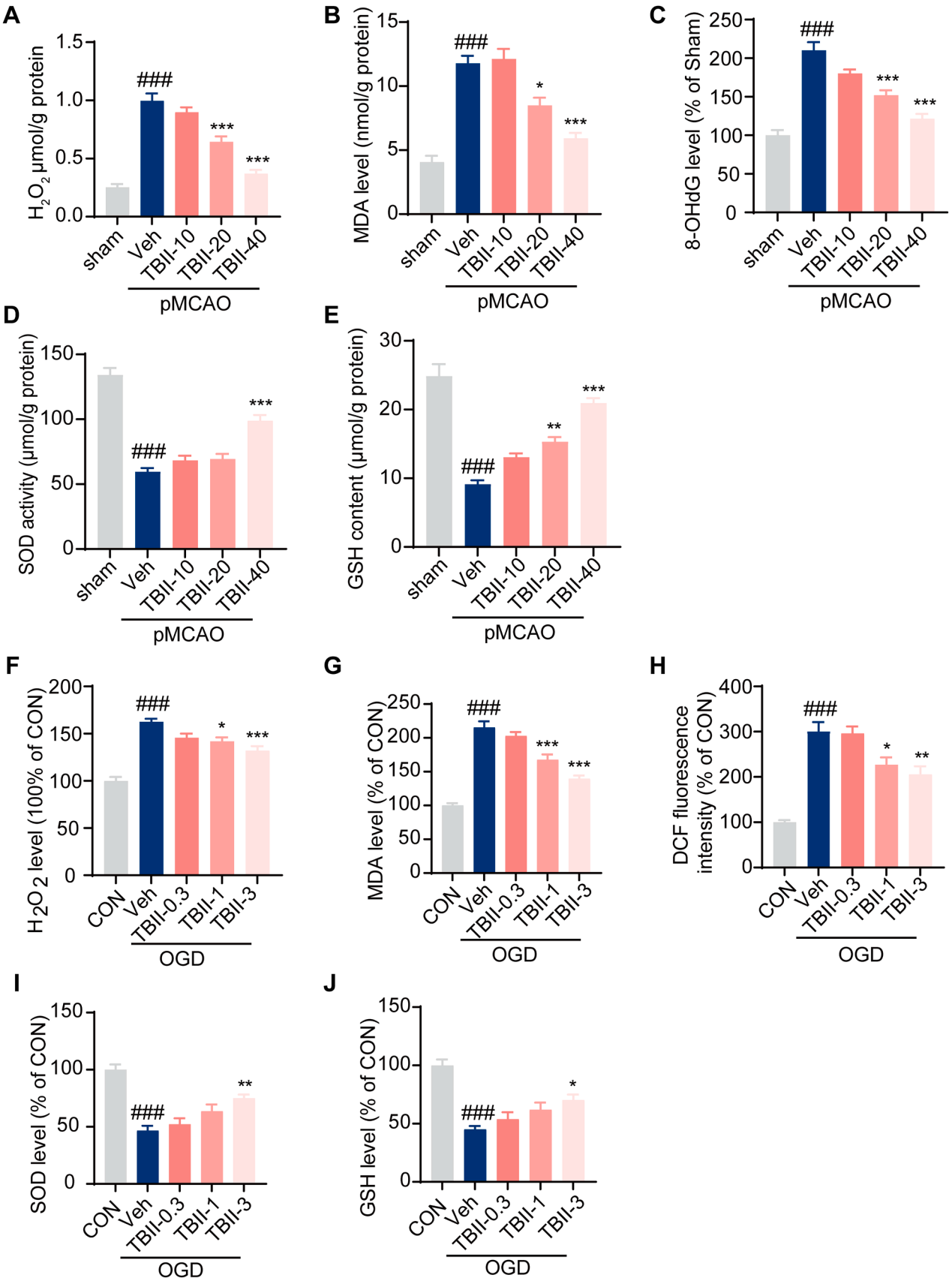

Fig. 2. TBII reduces oxidative stress in pMCAO-treated rats and OGD-treated HT22 cells. Oxidative stress markers in the ipsilateral cortex: (A) Hydrogen peroxide (H2O2), (B) malondialdehyde (MDA), (C) 8-hydroxy-2′-deoxyguanosine (8-OHdG), (D) superoxide dismutase (SOD) activity and (E) glutathione (GSH) content, n=4. Corresponding oxidative stress markers in HT22 cells: (F) H2O2, (G) MDA, (H) DCF fluorescence intensity, (I) SOD activity and (J) GSH content, n=6. ###p<0.001 vs. Sham or CON group; ***p<0.001, **p<0.01, *p<0.05 vs. pMCAO or OGD group.

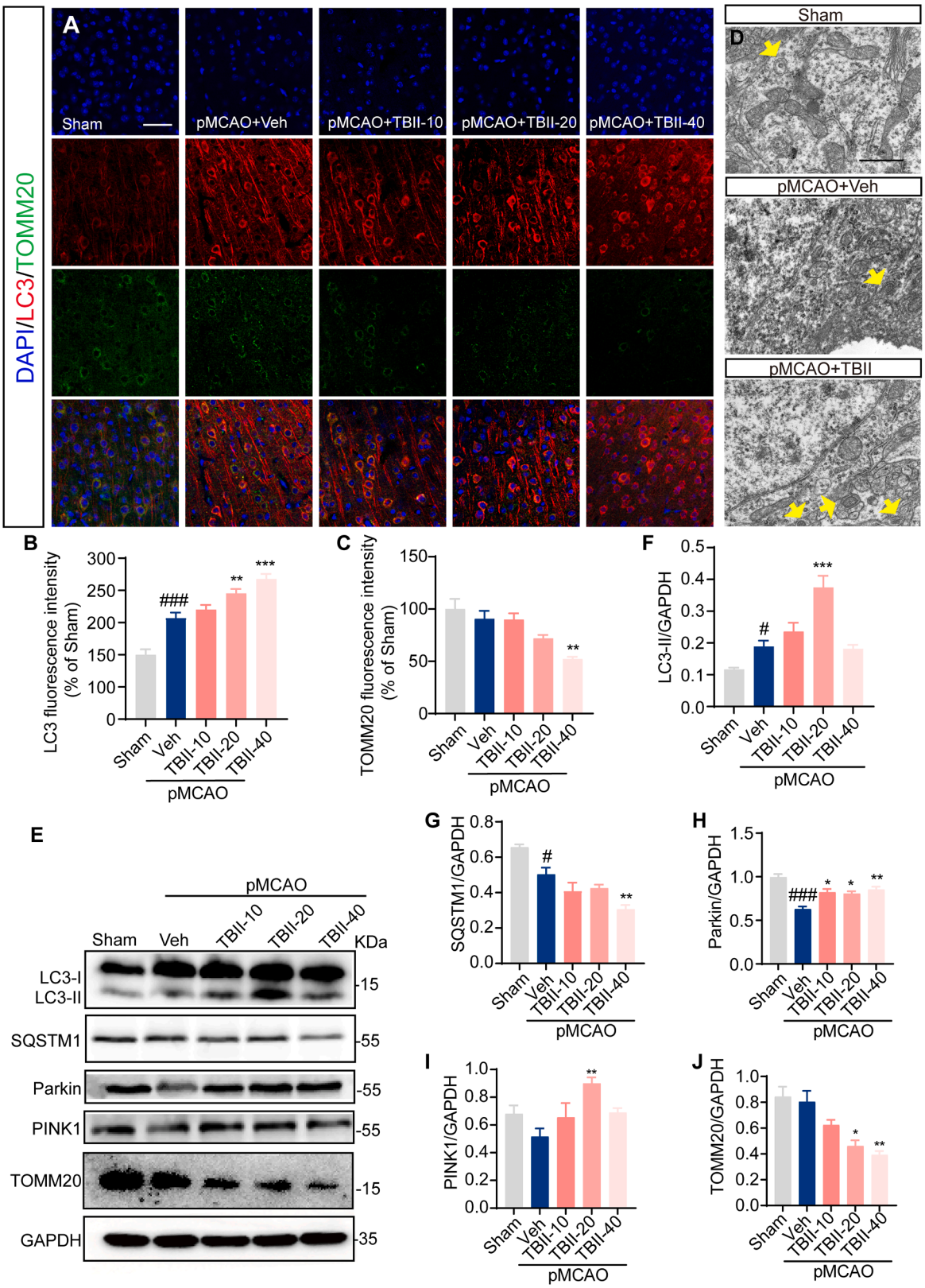

Fig. 3. TBII mitigates the impairment of mitophagy in the ipsilateral cortex at 24 h post-pMCAO. Representative fluorescence images (A) and quantitation of fluorescence intensity of LC3-labeled autophagosomes (B) and TOMM20-labeled mitochondria (C), n=6. Scale bar = 50 μm. (D) Representative transmission electron microscope (TEM) images (n=3), scale bar = 1 μm. (E-J) Protein expression of mitophagy-related markers: LC3, Sequestosome-1 (SQSTM1), PTEN-induced putative kinase 1 (PINK1), Parkin, and TOMM20 (n=3). GAPDH was used as a loading control. Data are represented as mean ± SEM. Statistical analysis was performed by one-way ANOVA with LSD test. ###p<0.001, #p<0.05 vs. Sham group; ***p<0.001, **p<0.01, *p<0.05 vs. pMCAO group.

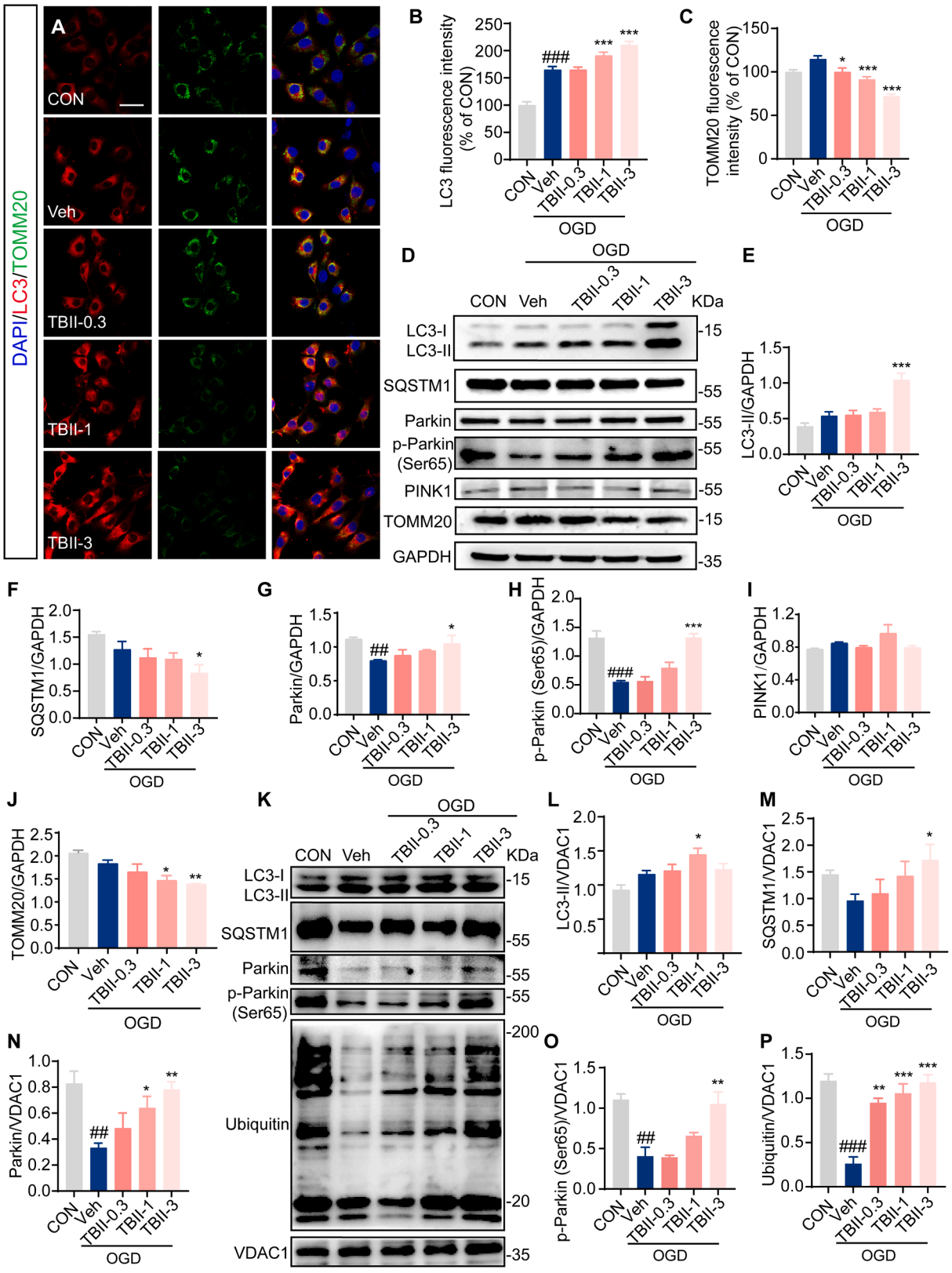

Fig. 4. TBII mitigates impaired mitophagy at 12 h after OGD in HT22 cells. Representative fluorescence images (A) and quantitation of fluorescence intensity of LC3-labeled autophagosomes (B) and TOMM20-labeled mitochondria (C). Scale bar = 20 μm, n=6. (D-J) Protein expression of autophagy- and mitophagy-related markers: LC3, SQSTM1, Parkin, p-Parkin (Ser65), PINK1, TOMM20 (n=3). (K-P) Protein level in mitochondrial extract: LC3, SQSTM1 and Parkin, p-Parkin (Ser65), Ubiquitin (n=3). Voltage-dependent anion-selective channel 1 (VDAC1) was used as a mitochondrial loading control. Data are represented as mean ± SEM. Statistical analysis was performed by one-way ANOVA with LSD test. ###p<0.001, ##p<0.01 vs. CON group; ***p<0.001, **p<0.01, *p<0.05 vs. OGD+Veh group.

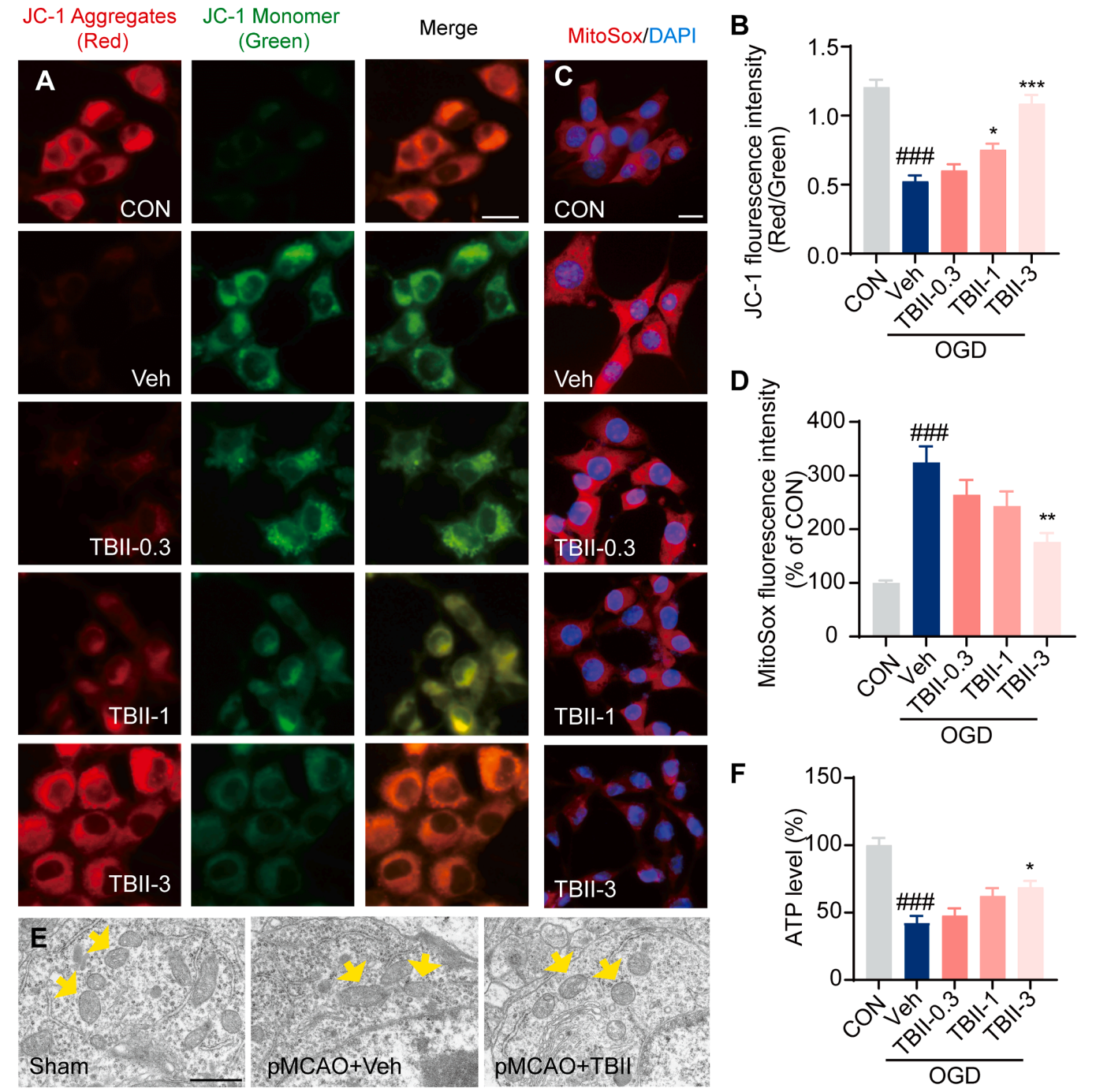

Fig. 5. TBII improves mitochondrial function following ischemic stroke (IS). (A-B) Mitochondrial membrane potential (MMP) assessed by JC-1 staining in OGD-treated HT22 cells. Scale bar = 20 μm. (C-D) Mitochondrial reactive oxygen species (ROS) production assessed by MitoSOX Red staining. Scale bar = 20 μm. (E) Mitochondrial ultrastructure visualized by TEM in the ipsilateral cortex at 24 h after pMCAO. Scale bar = 1 μm. (F) Intracellular ATP levels. n=6. Data are represented as mean ± SEM. Statistical analysis was performed by one-way ANOVA with LSD test. ###p<0.001, vs. CON group; ***p<0.001, **p<0.01, *p<0.05 vs. OGD group.

treatment prevented the OGD-induced reduction in ATP levels (Fig. 5F). Collectively, these results demonstrate that TBII preserves mitochondrial integrity and function while attenuating mitochondrial oxidative stress after IS.

TBII improves mitochondrial function and attenuates ischemic injury after IS through enhancing mitophagy

We used a mitophagy inhibitor Mdivi-1 to investigate whether TBII's beneficial effects on mitochondrial function and brain ischemic injury are mediated through mitophagy. In OGD-treated HT22 cells, treatment with Mdivi-1 reversed the TBII-mediated increase in the levels of MMP, GSH and ATP, SOD activity, and cell viability, and TBII-induced decrease in the levels of MitoSox fluorescence intensity, H_2O_2, MDA and DCF fluorescence intensity (Fig. 6A–K). Importantly, in pMCAO-operated mice, administration of Mdivi-1 abolished the therapeutic benefits of TBII on ischemic injury (Fig. 6L–O). These findings suggest that TBII-induced improvement of brain ischemic injury and mitochondrial function are primarily mediated through enhancing mitophagy.

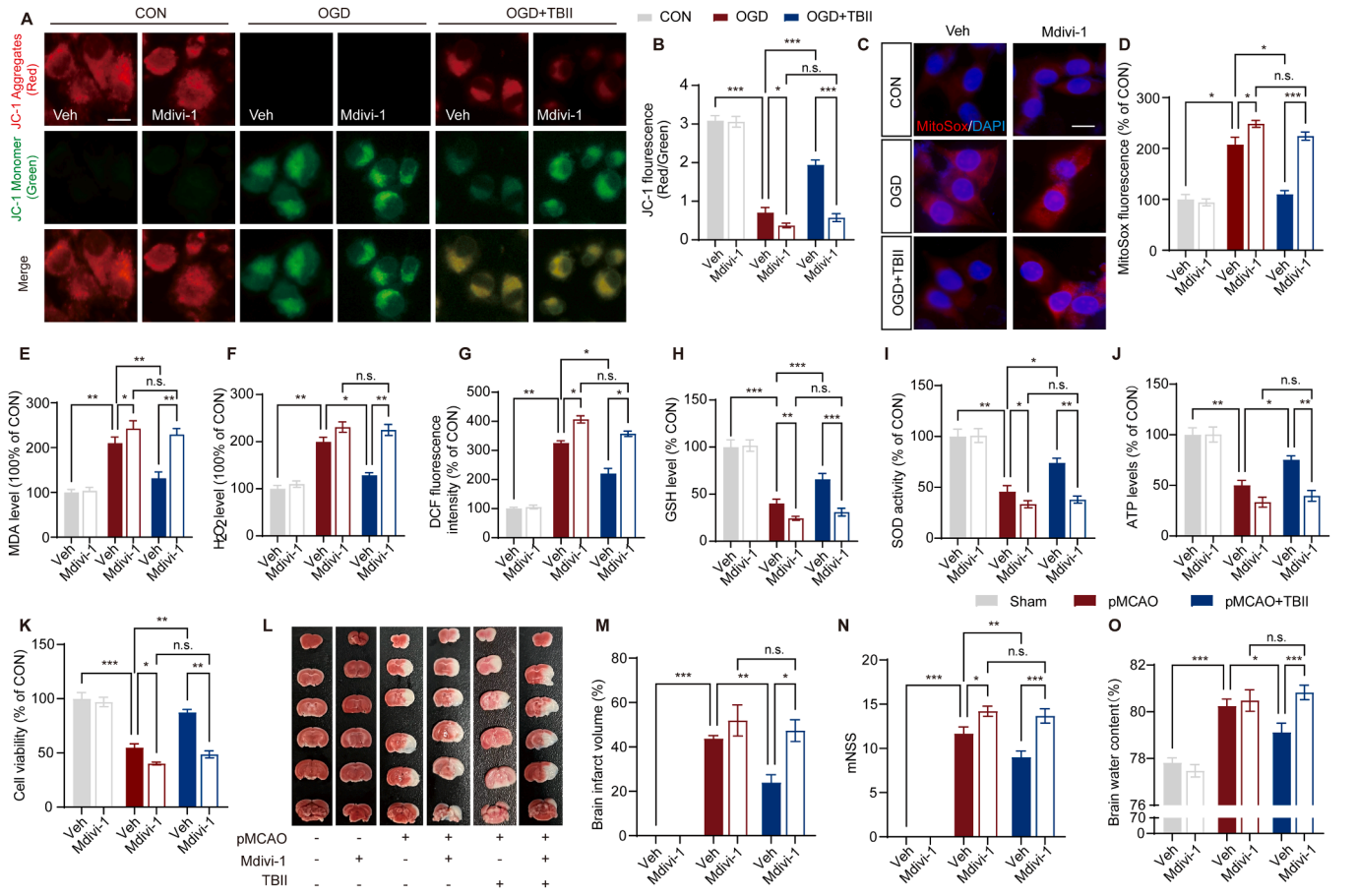

Fig. 6. TBII alleviates oxidative stress and IS injury through enhancing mitophagy. Mitochondrial membrane potential detected by JC-1 staining (A-B) and ROS detected by MitoSox staining (C-D) in OGD-treated HT22 cells treated with or without mitophagy inhibitor Mdivi-1(n=6). Scale bar = 20 μm. Oxidative stress markers: MDA (E), H2O2 (F) and DCF (G), antioxidant: GSH (H) and SOD (I), ATP level (J) and cell viability (K) in HT22 cells. n=4. (L-M) Cerebral infarct volume detected by TTC staining. Assessment of neurological function by mNSS (N) and brain water content (O) in pMCAO-operated mice treated with/without Mdivi-1. n=5-6. Data are represented as mean ± SEM. Statistical analysis was performed by two-way ANOVA with LSD test. ***p<0.001, **p<0.01, *p<0.05 vs. the indicated groups. ns, no significance.

Parkin is a potential target of TBII

To identify mitophagy-related targets of TBII, molecular docking was used to predict the binding affinity of TBII to autophagy related proteins. Parkin exhibited the highest docking score (-8.9 kcal/mol, supplementary Table 1). Structure analysis revealed the 3-position oxygen-β-D-pyran glucosyl moiety of TBII core forms a strong hydrogen bond with Gln178, while the 3-position oxygen-β-D-pyran galactosyl moiety interacts with key amino acids Asn428 and Lys435 via multiple hydrogen bonds. Additionally, the core 26-position oxygen-β-D-pyran glucosyl moiety establishes hydrogen bond interactions with Leu176 and Trp453. Furthermore, the steroid component engages in hydrophobic interactions with key residues, including Thr177, Gly179, and His433 (Fig. 7A).

Molecular dynamics simulations provided further insights into the hydrogen bond interactions between TBII and Parkin (Fig. 7B). Root mean square deviation (RMSD) analysis demonstrated that the Parkin-TBII complex exhibited sustained high structural deviation after 150 ns, exceeding the fluctuations observed in normal apo-Parkin range, suggesting sustained conformational rearrangement after ligand binding. Root mean square fluctuation (RMSF) profiling highlighted region-specific flexibility changes: the N-terminal ubiquitin-like domain (residues 0-76, highlighted in green) showed a 138% increase in flexibility, while the catalytic RING0 domain (residues 195-200, highlighted in black) displayed reduced fluctuations (-35%), suggesting that TBII binding destabilizes the autoinhibitory interface while stabilizing the catalytic core. Consistent with these observations, radius of gyration (Rg) measurements confirmed global expansion of the complex, with Parkin-TBII maintaining a 7.3% higher average Rg than apo-Parkin, particularly after 150 ns (Fig. 7B–E). This expansion was consistent with the RMSF/RMSD trends. This expansion supports transition to an open, catalytically competent state.

Moreover, CETSA results showed that TBII promoted Parkin thermal stability across multiple temperature gradients (Fig. 7F). DARTS assay further validates the molecular affinity between TBII and Parkin. The results showed that in comparison to the non-pronase group, the Parkin protein exhibited a remarkable reduction in the presence of pronase, while TBII protected Parkin from pronase degradation in a concentration-dependent manner (Fig. 7G). We also examined the binding affinity of TBII with ULK1 and LAMP1, which showed relatively higher and lower docking scores, using the CETSA method. As shown in Fig. S4A, B, TBII treatment significantly enhanced the thermal stability of ULK1, consistent with docking prediction, where it had only minimal effect on LAMP1. These findings support the molecular docking predictions, indicating a potential role of TBII in regulating mitophagy. Collectively, these findings provide compelling evidence that TBII directly interacts with the Parkin protein.

TBII attenuates ischemic injury after IS via Parkin to improve mitochondrial function

Having established Parkin as a potential target of TBII in improving

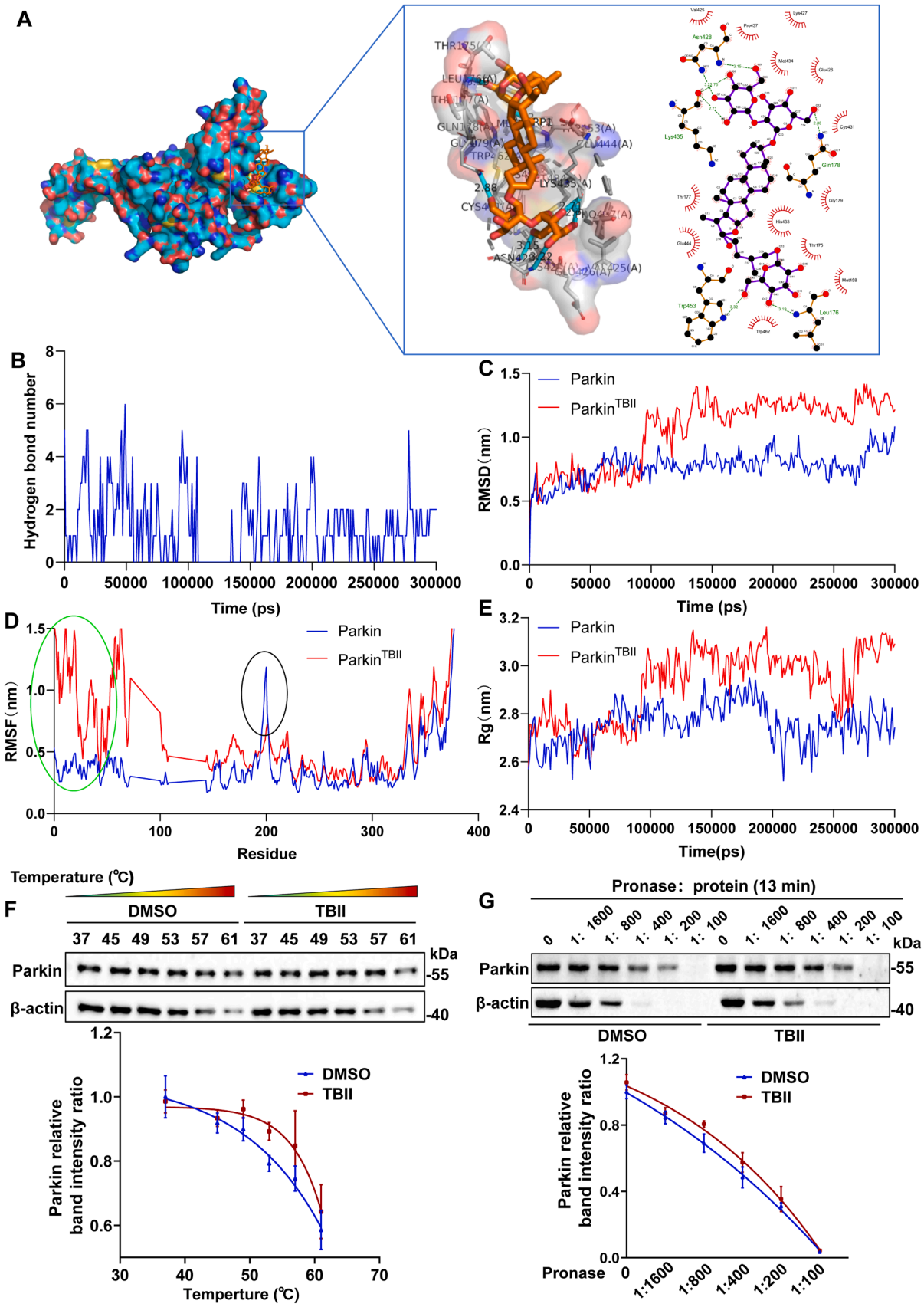

Fig. 7. Parkin is a molecular target of TBII. (A) Predicted the binding mode of Parkin with TBII from molecular docking analysis. Molecular dynamics simulation analysis showing the hydrogen bond number (B), root-mean-square deviation (RMSD, C), root-mean-square fluctuation (RMSF, D) and radius of gyration (Rg, E). Cellular thermal shift assays (CETSA, F) and drug affinity responsive target stability (DARTS, G) confirm that TBII enhances Parkin stability. n=4.

cerebral ischemic injury, we next investigated its role in mediating TBII therapeutic effects on ischemic injury and mitochondrial function. A LV delivery system encoding GFP and sh*Prkn* was constructed to knockdown Parkin in HT22 cells. Western blot analysis showed that Parkin expression significantly decreased in HT22 cells infected with LV-sh*Prkn*-3 compared to those injected with LV encoding GFP and a scramble shRNA (sh*Scr*, Fig. S5A and B). This indicate that LV-sh*Prkn*-3 can specifically downregulate Parkin expression, validating the knockout efficiency for subsequent experiments. Notably, the TBII-mediated decreased in MitoSox, H_2O_2 and MDA levels were reversed by Parkin knockdown (Fig. 8A–D). Conversely, TBII-mediated increase in the levels of GSH, SOD activity, ATP and cell viability were abolished by Parkin knockdown (Fig. 8E–H). Consistent with these *in vitro* findings, Parkin knockdown eliminated the therapeutic effects of TBII against ischemic injury *in vivo* (Fig. 8I to K). These findings indicate that Parkin is essential for TBII-mediated improvement of mitochondrial function and attenuation of ischemic injury after IS.

Discussion

The present study demonstrates for the first time that TBII exerts a significant anti-IS effect, likely through activating Parkin-dependent mitophagy pathway, which facilitates the degradation of damaged mitochondria, improves mitochondrial function, and ultimately suppresses mitochondrial oxidative stress (Fig. 9).

It has been reported that TBII possesses favorable water solubility and stability. The pharmacokinetic parameters of TBII, including its absorption, distribution, metabolism, and excretion (ADME) in rats, have been reported in literature (Cai et al., 2008; Feng et al., 2014; Jia et al., 2015; Liu et al., 2012; Xu et al., 2014). Although pharmacokinetic studies indicate that TBII has low absolute bioavailability (1.1%) and limited blood-brain barrier penetration, it exhibits diverse neuroprotective effects. It has been shown to alleviate learning and memory deficits in multiple dementia models, including those induced by MCAO, scopolamine, LPS, and Aβ, establishing its potential for treating central nervous system disorders (Chen et al., 2020; Li et al., 2007; Ouyang et al., 2005; Zhao et al., 2016). Excitingly, the present study identifies a novel beneficial effect of TBII in the treatment of IS, evidenced by a significant reduction in brain infarct volume, brain edema, and neurological deficits, particularly in motor function. In this study, we select the dosage of TBII (5-80 mg/kg, i.g.) based on previous studies (Deng et al., 2015; Li et al., 2007; Xing et al., 2020; Zhao et al., 2016) and toxicological data indicating no toxicity below 180 mg/kg in rats (Lin et al., 2017). To ensure consistency in the route of administration, we selected clinically approved NBP as the positive control. Our findings revealed that TBII exerts therapeutic effects against cerebral ischemia within the dose range of 10-80 mg/kg in a dose-dependent manner. The efficacy observed at 40 and 80 mg/kg was comparable, indicating that 40 mg/kg represents the maximal effective dose. Consequently, a dose range of 10-40 mg/kg for subsequent mechanistic investigations. Importantly, the effective dose of TBII (10 mg/kg) was markedly lower than that of NBP (80 mg/kg). Consistently, TBII (0.3-10 μM) reduced cell death in OGD-treated HT22 cells in a concentration-dependent manner, confirming its efficacy both *in vivo* and *in vitro*.

It has been shown that TBII's efficacy in improving central nervous system disorders may involve alleviating oxidative stress (Huang et al., 2012; Xie et al., 2018; Zhao et al., 2016). Notably, IS triggers mitochondrial damage, resulting in excessive mitochondrial reactive oxygen species production. Oxidative stress represents a central pathological mechanism in IS, contributing to neuroinflammation, neuronal apoptosis, and the blood-brain barrier disruption, all of which exacerbate cerebral ischemic injury (Lochhead et al., 2024). Excessive reactive oxygen species generation activates adhesion molecules and promote immune cell infiltration, lipid peroxidation, and neuronal apoptosis. Therefore, therapeutic strategies that reduce the production of free radicals or enhance their clearance may confer neuroprotection against ischemic brain damage (Akhtar et al., 2025). Antioxidant enzymes, such as SOD, function as key enzymatic regulators that maintain redox homeostasis. These enzymes protect against oxidative damage by enhancing free radical scavenging, reducing MDA levels, and thereby attenuating lipid peroxidation and ischemic injury (Zhao et al., 2024). Our study demonstrates that TBII treatment significantly decreased MDA, H_2O_2, and intracellular reactive oxygen species, while increasing GSH levels and SOD activity following IS. These findings suggest that the neuroprotective effects of TBII against cerebral ischemic injury are mediated, at least in part, through suppressing oxidative stress.

Recent studies indicate that timosaponin compounds, including TBII and TAIII, can significantly activate autophagy (Lok et al., 2011; Wang et al., 2021), though its role in regulating autophagy abnormalities after IS remains unclear. Although autophagy and mitophagy play complex roles in ischemic injury, their effects appear context-dependent. Non-selective autophagy can be detrimental by indiscriminately degrading cellular compartments, which may be harmful (Zhou et al., 2023), where selective autophagy, especially mitophagy, can exert ischemic protective effects by promoting the degradation of damaged mitochondria (Li et al., 2023a). We have previously reported that IS induces dynamic changes in autophagy, with early moderate activation followed by late impaired autophagic flux, and found that enhancing both stages confer neuroprotection (Liu et al., 2019). Where similar dynamics for mitophagy after IS have not been described. In this study, we observed impaired mitophagy after pMCAO and OGD, as indicated by increased LC3 without significant reduction in TOMM20. Notably, we administered TBII for seven days prior to pMCAO. This pre-treatment protocol was designed to ensure that TBII-induced enhancement of mitophagy was fully engaged at the very onset of the ischemic event. Our data demonstrate that this pre-emptive administration successfully mitigated the post-ischemic impairment of mitophagy and was associated with significant neuroprotection. The mitophagy inhibitor Mdivi-1 reversed TBII's benefits on mitochondrial function and oxidative stress and cerebral ischemic injury. These findings suggest that TBII alleviates ischemic injury by enhancing mitophagy and improving mitochondrial function.

Mitophagy is regulated through two distinct pathways: the PINK1/Parkin-mediated ubiquitination-dependent pathway and the ubiquitination-independent pathway. In the former, damaged mitochondria accumulate PINK1 on the outer mitochondrial membrane, which recruits Parkin (an E3 ubiquitin ligase) to ubiquitinate mitochondrial membrane proteins (Picca et al., 2023). This process enables autophagy receptor proteins like SQSTM1 to recognize damaged mitochondria for degradation (Li et al., 2023b). In the latter pathway, receptors such as BNIP3, NIX, and FUNDC1, directly bind to LC3 to promote the fusion of damaged mitochondria with autophagosomes (Wu et al., 2021b). Specifically, we found that TBII significantly upregulated PINK1 and Parkin expression following cerebral ischemia, while it had no effect on other mitophagy receptors, including BNIP3, NIX, and FUNDC1. Additionally, TBII upregulated the p-Parkin (Ser65) and promoted it translocate to mitochondria after IS. These findings suggest that TBII specifically regulates Parkin-mediated mitophagy by enhancing Parkin's ubiquitin ligase activity and promoting its recruitment to mitochondria. Importantly, molecular docking also revealed a strong binding affinity between TBII and Parkin. Subsequent CESTA and DARTS assay further confirmed that TBII bind to and stabilize Parkin. Functional validation using Parkin knockdown (sh*Prkn*) demonstrated that Parkin knockdown abolished TBII's beneficial effects on mitochondrial function, oxidative stress, and ischemic injury. These results strongly suggest that TBII exerts its neuroprotective effects primarily through promoting Parkin-mediated mitophagy activation.

This study has certain limitations. First, this study did not directly determine whether TBII can cross the blood-brain barrier after cerebral ischemia. However, previous pharmacokinetic studies have detected low levels of TBII in brain tissue following oral administration (Xu et al., 2014). Numerous studies, including our own study, have shown

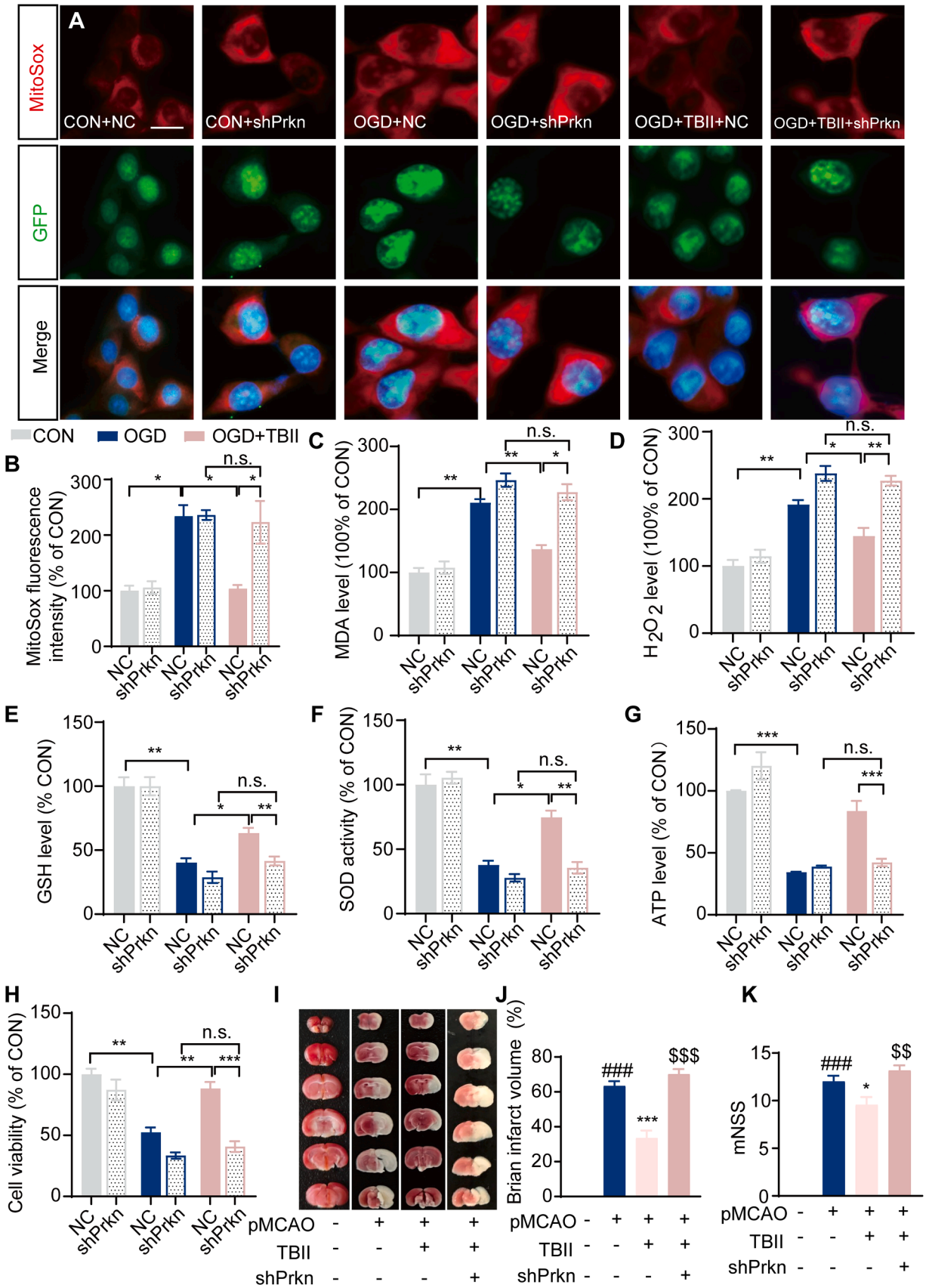

Fig. 8. TBII mitigates oxidative stress and ischemic injury by targeting Parkin. Effects of TBII and Parkin knockdown (shPrkn) on mitochondrial ROS (A-B), oxidative stress markers (C-D), antioxidants (E-F), ATP (G), and cell viability (H) in OGD-treated HT22 cells Scale bar = 20 μm. n=4. Effects of TBII and Parkin knockdown on cerebral infarct volume (I-J) and neurological function (K) in pMCAO-operated mice. n=7-9. Data are represented as mean ± SEM. Statistical analysis was performed by one-way ANOVA with LSD test. ***p<0.001, **p<0.01, *p<0.05 vs. the indicated groups. n.s., no significance.

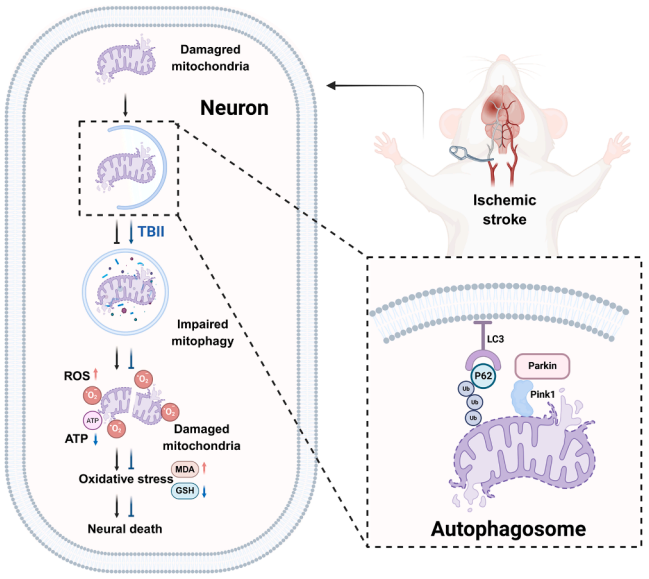

Fig. 9. Schematic of TBII's protective mechanisms against cerebral ischemic injury. Cerebral ischemia reduces Parkin levels, impairing mitophagy and leading to the accumulation of damaged mitochondria within neurons. This mitochondrial dysfunction results in decreased MMP and intracellular ATP production, alongside excessive mitochondrial ROS, resulting oxidative stress is evidenced by increased MDA levels and decreased GSH levels, ultimately exacerbating neuronal injury. Notably, TBII (blue effect) counteracts this by stabilizing Parkin and enhancing its expression and activity. This promotes the clearance of accumulation of damaged mitochondria via mitophagy and reduces oxidative stress, and ultimately attenuating cerebral ischemic injury. This image was created in BioRender (https://BioRender.com/q28av82).

therapeutic efficacy in multiple neurological disorders (Chen et al., 2020; Li et al., 2007; Zhao et al., 2016). This may be due to blood-brain barrier disruption during pathological conditions, particularly in cerebral ischemia, or TBII protective effects through its metabolites. Notably, it has been shown that TBII is biotransformation to TAIII (Jia et al., 2015; Liu et al., 2012), a neuroprotective saponin known to modulate autophagy, which could contribute to its effects. Second, CETSA and DARTS confirm a physical TBII-Parkin interaction, though quantitative methods like surface plasmon resonance are needed for precise characterization. We also validate that TBII significantly enhances the thermal stability of ULK1 while having a minimal effect on the low-scoring protein LAMP1, confirming that TBII's interactions are specific. This compelling finding suggests that TBII's role may extend to broader autophagic pathways. However, to maintain a clear and focused narrative on the novel Parkin-dependent mitophagy pathway, ULK1 is not pursued further, a recognized limitation that opens compelling avenues for future research. Moreover, as mitophagy and macroautophagy involve distinct pathways, the influence of TBII on macroautophagy was not explored here and remains a subject for our future investigations.

These findings and limitations directly inform a clear path forward. Future research should prioritize developing novel formulations, such as nanoparticle carriers or nasal hydrogels (Chen et al., 2020), to enhance TBII's brain bioavailability and fully realize its therapeutic potential. Furthermore, our work solidifies the activation of Parkin-mediated mitophagy as a compelling therapeutic strategy for IS. This paves the way for developing next-generation neuroprotectants that specifically target this pathway, not only for stroke but also for other neurological disorders characterized by mitochondrial dysfunction.

In conclusion, this study is the first to demonstrate that TBII alleviates acute cerebral ischemic injury by enhancing Parkin-mediated mitophagy and inhibiting mitochondrial oxidative stress. Mechanistically, IS caused the impairment of mitophagy that prevents the clearance of damaged mitochondria, leading to accumulated reactive oxygen species in mitochondria and subsequent oxidative stress. TBII directly binds to and stabilizes Parkin, initiating a cascade of ubiquitination events that recruited to mitochondria. This rescued mitophagy eliminates reactive oxygen species-generating mitochondria, reducing oxidative stress and preserving mitochondrial function. Thus, TBII attenuates ischemic brain injury by enhancing Parkin-dependent mitophagy.

CRediT authorship contribution statement

Yueyang Liu: Writing – original draft, Supervision. **Hanxiao Shang:** Formal analysis, Data curation. **Lu Zhang:** Methodology, Investigation. **Rong Fu:** Methodology, Investigation. **Yayi Li:** Methodology, Investigation. **Zhuo Wang:** Methodology, Investigation. **Yanru Zhen:** Methodology, Investigation. **Qi Zhang:** Methodology, Investigation. **Yang Zhao:** Formal analysis, Data curation, Conceptualization. **Guannan Wang:** Writing – review & editing. **Ming-Sheng Zhou:** Writing – review & editing, Supervision, Conceptualization.

Declaration of competing interest

The authors declare no conflicts of interest.

Acknowledgement

This project was supported by the National Natural Science Foundation of China (82270434, 81970357) to Ming-sheng Zhou, the National Natural Science Foundation of China (82100316) to Lu Zhang and the National Natural Science Foundation of China (82574406), Key R&D Project of Liaoning Provincial Department of Science and Technology (2025JH2/101300019), the U35 Outstanding Young Talent Program of Shenyang (RC240612) and the Research Project of Educational Commission of Liaoning Province (LJ212410164003) to Yueyang Liu.

Supplementary materials

Supplementary material associated with this article can be found, in the online version, at doi:10.1016/j.phymed.2025.157580.

References

Akhtar, W., Muazzam Khan, M., Kumar, S., Ahmad, U., Husen, A., Avirmed, S., 2025. Pathophysiology of cerebral ischemia-reperfusion injury: an overview of oxidative stress and plant-based therapeutic approaches. Brain Res. 1847, 149308.
Cai, F., Sun, L., Gao, S., Yang, Y., Yang, Q., Chen, W., 2008. A rapid and sensitive liquid chromatography-tandem mass spectrometric method for the determination of timosaponin B-II in blood plasma and a study of the pharmacokinetics of saponin in the rat. J. Pharm. Biomed. Anal. 48, 1411–1416.
Chen, W., Li, R., Zhu, S., Ma, J., Pang, L., Ma, B., Du, L., Jin, Y., 2020. Nasal timosaponin BII dually sensitive in situ hydrogels for the prevention of Alzheimer's disease induced by lipopolysaccharides. Int. J. Pharm. 578, 119115.
Connelly, E.M., Frankel, K.S., Shaw, G.S., 2023. Parkin and mitochondrial signalling. Cell Signal. 106, 110631.
Deng, X.Y., Chen, J.J., Li, H.Y., Ma, Z.Q., Ma, S.P., Fu, Q., 2015. Cardioprotective effects of timosaponin B II from Anemarrhenae asphodeloides Bge on isoproterenol-induced myocardial infarction in rats. Chem. Biol. Interact. 240, 22–28.
Duan, W.L., Gu, L.H., Guo, A., Wang, X.J., Ding, Y.Y., Zhang, P., Zhang, B.G., Li, Q., Yang, L.X., 2025. Molecular mechanisms of programmed cell death and potential targeted pharmacotherapy in ischemic stroke (Review). Int. J. Mol. Med. 56, 103.
Feng, Y., Chen, B., Lin, A., Liu, Y., 2014. Simultaneous determination of timosaponin B-II and A-III in rat plasma by LC-MS/MS and its application to pharmacokinetic study. J. Chromatogr. B Analyt. Technol. Biomed. Life Sci. 965, 119–126.
Huang, J.F., Shang, L., Liu, P., Zhang, M.Q., Chen, S., Chen, D., Fan, C.L., Wang, H., Xiong, K., 2012. Timosaponin-BII inhibits the up-regulation of BACE1 induced by ferric chloride in rat retina. BMC Complement. Altern. Med. 12, 189.
Jia, Y., Fu, Z., Li, Z., Hu, P., Xue, R., Chen, M., Xiang, T., Huang, C., 2015. In-vivo and in-vitro metabolism study of timosaponin B-II Using HPLC-ESI-MSn. Chromatographia 78, 1175–1184.
Lee, B., Jung, K., Kim, D.H., 2009. Timosaponin AIII, a saponin isolated from Anemarrhena asphodeloides, ameliorates learning and memory deficits in mice. Pharmacol. Biochem. Behav. 93, 121–127.
Li, J., Wu, J., Zhou, X., Lu, Y., Ge, Y., Zhang, X., 2023. Targeting neuronal mitophagy in ischemic stroke: an update. Burns Trauma 11 tkad018.

Li, T.J., Qiu, Y., Yang, P.Y., Rui, Y.C., Chen, W.S., 2007. Timosaponin B-II improves memory and learning dysfunction induced by cerebral ischemia in rats. Neurosci. Lett. 421, 147–151.
Lin, N., Liu, B., Zhang, J., Long, Y., Dong, G., Jin, H., Ma, B., 2017. Acute toxicity, 28-day repeated-dose toxicity and toxicokinetic study of timosaponin BII in rats. Regul. Toxicol. Pharmacol. 90, 244–257.
Liu, X., Xiang, D., Jin, W., Zhao, G., Li, H., Xie, B., Gu, X., 2022. Timosaponin B-II alleviates osteoarthritis-related inflammation and extracellular matrix degradation through inhibition of mitogen-activated protein kinases and nuclear factor-kappaB pathways in vitro. Bioengineered 13, 3450–3461.
Liu, Y., Che, X., Yu, X., Shang, H., Cui, P., Fu, X., Lu, X., Liu, Y., Wu, C., Yang, J., 2023. Phosphorylation of STAT3 at Tyr705 contributes to TFEB-mediated autophagy-lysosomal pathway dysfunction and leads to ischemic injury in rats. Cell Mol. Life Sci. 80, 160.
Liu, Y., Che, X., Zhang, H., Fu, X., Yao, Y., Luo, J., Yang, Y., Cai, R., Yu, X., Yang, J., Zhou, M.S., 2021. CAPN1 (Calpain1)-mediated impairment of autophagic flux contributes to cerebral ischemia-induced neuronal damage. Stroke 52, 1809–1821.
Liu, Y., Liu, Q., Shang, H., Li, J., Chai, H., Wang, K., Guo, Z., Luo, T., Liu, S., Liu, Y., Wang, X., Zhang, H., Wu, C., Song, S.J., Yang, J., 2024. Potential application of natural compounds in ischaemic stroke: focusing on the mechanisms underlying "lysosomocentric" dysfunction of the autophagy-lysosomal pathway. Pharmacol. Ther. 263, 108721.
Liu, Y., Xue, X., Zhang, H., Che, X., Luo, J., Wang, P., Xu, J., Xing, Z., Yuan, L., Liu, Y., Fu, X., Su, D., Sun, S., Zhang, H., Wu, C., Yang, J., 2019. Neuronal-targeted TFEB rescues dysfunction of the autophagy-lysosomal pathway and alleviates ischemic injury in permanent cerebral ischemia. Autophagy 15, 493–509.
Liu, Z., Zhu, D., Lv, L., Li, Y., Dong, X., Zhu, Z., Chai, Y., 2012. Metabolism profile of timosaponin B-II in urine after oral administration to rats by ultrahigh-performance liquid chromatography/quadrupole-time-of-flight mass spectrometry. Rapid Commun. Mass Spectrom. 26, 1955–1964.
Lochhead, J.J., Ronaldson, P.T., Davis, T.P., 2024. The role of oxidative stress in blood-brain barrier disruption during ischemic stroke: antioxidants in clinical trials. Biochem. Pharmacol. 228, 116186.
Lok, C.N., Sy, L.K., Liu, F., Che, C.M., 2011. Activation of autophagy of aggregation-prone ubiquitinated proteins by timosaponin A-III. J. Biol. Chem. 286, 31684–31696.
Longa, E.Z., Weinstein, P.R., Carlson, S., Cummins, R., 1989. Reversible middle cerebral artery occlusion without craniectomy in rats. Stroke 20, 84–91.
Lu, W.Q., Qiu, Y., Li, T.J., Tao, X., Sun, L.N., Chen, W.S., 2009. Timosaponin B-II inhibits pro-inflammatory cytokine induction by lipopolysaccharide in BV2 cells. Arch. Pharm. Res. 32, 1301–1308.
Lu, Y., Li, Z., Zhang, S., Zhang, T., Liu, Y., Zhang, L., 2023. Cellular mitophagy: mechanism, roles in diseases and small molecule pharmacological regulation. Theranostics 13, 736–766.
Majumder, D., 2024. Ischemic stroke: pathophysiology and evolving treatment approaches. Neurosci. Insights 19, 26331055241292600.
Meng, Q., Liu, Q., Mi, Y., Xu, L., Wang, F., Mu, D., Liu, Y., Yang, Y., Huang, Y., He, D., Hou, Y., 2025a. Multi-dimensional data-driven computational drug repurposing strategy for screening novel neuroprotective agents in ischemic stroke. Theranostics 15, 7653–7676.
Meng, Q., Mi, Y., Xu, L., Liu, Y., Liang, D., Wang, Y., Wang, Y., Liu, Y., Chen, G., Hou, Y., 2025b. A quinolinyl analog of resveratrol improves neuronal damage after ischemic stroke by promoting Parkin-mediated mitophagy. Chin. J. Nat. Med. 23, 214–224.
Mi, Y., Wang, Y., Liu, Y., Dang, W., Xu, L., Tan, S., Liu, L., Chen, G., Liu, Y., Li, N., Hou, Y., 2024. Kellerin alleviates cerebral ischemic injury by inhibiting ferroptosis via targeting Akt-mediated transcriptional activation of Nrf2. Phytomedicine 128, 155406.
Nixon, R.A., Rubinsztein, D.C., 2024. Mechanisms of autophagy-lysosome dysfunction in neurodegenerative diseases. Nat. Rev. Mol. Cell Biol. 25, 926–946.
Ouyang, S., Sun, L.S., Guo, S.L., Liu, X., Xu, J.P., 2005. Effects of timosaponins on learning and memory abilities of rats with dementia induced by lateral cerebral ventricular injection of amyloid beta- peptide. Di Yi Jun Yi Da Xue Xue Bao 25, 121–126.
Picca, A., Faitg, J., Auwerx, J., Ferrucci, L., D'Amico, D., 2023. Mitophagy in human health, ageing and disease. Nat. Metab. 5, 2047–2061.
Qin, C., Yang, S., Chu, Y.H., Zhang, H., Pang, X.W., Chen, L., Zhou, L.Q., Chen, M., Tian, D.S., Wang, W., 2022. Signaling pathways involved in ischemic stroke: molecular mechanisms and therapeutic interventions. Signal Transduct. Target. Ther. 7, 215.
Sun, E., Zhang, J., Deng, Y., Wang, J., Wu, Q., Chen, W., Ma, X., Chen, S., Xiang, X., Chen, Y., Wu, T., Yang, Y., Chen, B., 2022. Docosahexaenoic acid alleviates brain damage by promoting mitophagy in mice with ischaemic stroke. Oxid. Med. Cell Longev. 2022, 3119649.
Tang, J., Hu, Z., Tan, J., Yang, S., Zeng, L., 2016. Parkin protects against oxygen-glucose deprivation/reperfusion insult by promoting Drp1 degradation. Oxid. Med. Cell Longev., 8474303, 2016.
Wang, N., Xu, P., Wu, R., Wang, X., Wang, Y., Shou, D., Zhang, Y., 2021. Timosaponin BII improved osteoporosis caused by hyperglycemia through promoting autophagy of osteoblasts via suppressing the mTOR/NFkappaB signaling pathway. Free Radic. Biol. Med. 171, 112–123.
Wen, H., Li, L., Zhan, L., Zuo, Y., Li, K., Qiu, M., Li, H., Sun, W., Xu, E., 2021. Hypoxic postconditioning promotes mitophagy against transient global cerebral ischemia via PINK1/Parkin-induced mitochondrial ubiquitination in adult rats. Cell Death Dis. 12, 630.
Wu, W., Xu, L., Sun, L., Xue, J., Wang, F., Guo, H., Lei, N., Liu, D., Liu, Y., Liang, D., Wang, Y., Mi, Y., Chai, H., Hou, Y., 2025a. Ethanol extract of *Periploca forrestii* Schltr. and chlorogenic acid alleviate ischemic stroke by inhibiting TLR4-mediated neuroinflammation. Phytomedicine 145, 157026.
Wu, X., Zheng, Y., Liu, M., Li, Y., Ma, S., Tang, W., Yan, W., Cao, M., Zheng, W., Jiang, L., Wu, J., Han, F., Qin, Z., Fang, L., Hu, W., Chen, Z., Zhang, X., 2021. BNIP3L/NIX degradation leads to mitophagy deficiency in ischemic brains. Autophagy 17, 1934–1946.
Wu, Y., Li, Z., Ding, T., Yang, Y., Wei, C., Zhang, S., Fan, X., 2025b. Bidirectional regulation of neuronal autophagy in ischemic stroke: mechanisms and therapeutic potential. Ageing Res. Rev. 111, 102842.
Xie, Q., Zhao, H., Li, N., Su, L., Xu, X., Hong, Z., 2018. Protective effects of timosaponin BII on oxidative stress damage in PC12 cells based on metabolomics. Biomed. Chromatogr. 32, e4321.
Xing, N., Wang, Y., Wang, W., Zhong, R., Xia, T., Ding, Z., Yang, Y., Zhong, Y., Shu, Z., 2020. Cardioprotective effect exerted by Timosaponin BII through the regulation of endoplasmic stress-induced apoptosis. Phytomedicine 78, 153288.
Xu, Z., Gao, S., Cai, F., Zhang, F., Jiang, W., Liu, X., Chen, W., 2014. A novel LC-MS/MS method for determination of tissue distribution and excretion of timosaponin B-II in rat biological matrices. Biomed. Chromatogr. 28, 1011–1016.
Ye, X.C., Hao, Q., Ma, W.J., Zhao, Q.C., Wang, W.W., Yin, H.H., Zhang, T., Wang, M., Zan, K., Yang, X.X., Zhang, Z.H., Shi, H.J., Zu, J., Raza, H.K., Zhang, X.L., Geng, D.Q., Hu, J.X., Cui, G.Y., 2020. Dectin-1/Syk signaling triggers neuroinflammation after ischemic stroke in mice. J. Neuroinflammation 17, 17.
Zhang, T., Wang, J., Wang, S., Ma, C., 2015. Timosaponin B-II inhibits lipopolysaccharide-induced acute lung toxicity via TLR/NF-kappaB pathway. Toxicol. Mech. Methods 25, 665–671.
Zhang, X., Yan, H., Yuan, Y., Gao, J., Shen, Z., Cheng, Y., Shen, Y., Wang, R.R., Wang, X., Hu, W.W., Wang, G., Chen, Z., 2013. Cerebral ischemia-reperfusion-induced autophagy protects against neuronal injury by mitochondrial clearance. Autophagy 9, 1321–1333.
Zhao, C., Bai, X., Wen, A., Wang, J., Ding, Y., 2024. The therapeutic effects of salvianolic acids on ischemic stroke: from molecular mechanisms to clinical applications. Pharmacol. Res. 210, 107527.
Zhao, X., Liu, C., Qi, Y., Fang, L., Luo, J., Bi, K., Jia, Y., 2016. Timosaponin B-II ameliorates scopolamine-induced cognition deficits by attenuating acetylcholinesterase activity and brain oxidative damage in mice. Metab. Brain Dis. 31, 1455–1461.
Zhou, Z., Zhang, Y., Han, F., Chen, Z., Zheng, Y., 2023. Umbelliferone protects against cerebral ischemic injury through selective autophagy of mitochondria. Neurochem. Int. 165, 105520.